Acta Pharmacologica Sinica

ARTICLE

Aspirin triggers ferroptosis in hepatocellular carcinoma cells through restricting NF-κB p65-activated SLC7A11 transcription

Yu-fei Wang[1,2], Jin-yan Feng[2,3], Li-na Zhao[1,2], Man Zhao[4], Xian-fu Wei[2,3], Yu Geng[4], Hong-feng Yuan[1,2], Chun-yu Hou[1,2], Hui-hui Zhang[1,2], Guo-wen Wang[2,3]✉, Guang Yang[1,2]✉ and Xiao-dong Zhang[1,2]✉

A number of studies have shown that aspirin, as commonly prescribed drug, prevents the development of hepatocellular carcinoma (HCC). Ferroptosis as a dynamic tumor suppressor plays a vital role in hepatocarcinogenesis. In this study we investigated whether aspirin affected ferroptosis in liver cancer cells. RNA-seq analysis revealed that aspirin up-regulated 4 ferroptosis-related drivers and down-regulated 5 ferroptosis-related suppressors in aspirin-treated HepG2 cells. Treatment with aspirin (4 mM) induced remarkable ferroptosis in HepG2 and Huh7 cells, which was enhanced by the ferroptosis inducer erastin (10 μM). We demonstrated that NF-κB p65 restricted ferroptosis in HepG2 and Huh7 cells through directly binding to the core region of *SLC7A11* promoter and activating the transcription of ferroptosis inhibitor SLC7A11, whereas aspirin induced ferroptosis through inhibiting NF-κB p65-activated SLC7A11 transcription. Overexpression of p65 rescued HepG2 and Huh7 cells from aspirin-induced ferroptosis. HCC patients with high expression levels of SLC7A11 and p65 presented lower survival rate. Functionally, NF-κB p65 blocked the aspirin-induced ferroptosis in vitro and in vivo, which was attenuated by erastin. We conclude that aspirin triggers ferroptosis by restricting NF-κB-activated SLC7A11 transcription to suppress the growth of HCC. These results provide a new insight into the mechanism by which aspirin regulates ferroptosis in hepatocarcinogenesis. A combination of aspirin and ferroptosis inducer may provide a potential strategy for the treatment of HCC in clinic.

Keywords: hepatocellular carcinoma; aspirin; ferroptosis; NF-κB; SLC7A11; erastin; ferrostatin-1; PDTC

Acta Pharmacologica Sinica (2023) 44:1712–1724; https://doi.org/10.1038/s41401-023-01062-1

INTRODUCTION

Ferroptosis is an emerging type of cell death induced by metal iron and reactive oxygen species (ROS) and driven by lipid peroxidation [1, 2]. Among the core regulatory components, the cystine-glutamate antiporter known as system Xc^- or xCT (SLC7A11, encoded by the gene *SLC7A11*) imports cystine for the de novo synthesis of the important antioxidant peptide glutathione (GSH) [3, 4]. GSH, among many functions, is also used as a substrate of phospholipid hydroxyperoxide glutathione peroxidase (GPX4) to catalyze the detoxification of phospholipid hydroperoxides [5, 6]. Hence, ferroptosis can be potently induced by cysteine deprivation and GPX4 inhibition. Small pharmacological inhibitors, including the GPX4 inhibitor RSL3 and erastin as direct inhibitors of xCT-mediated import function, are widely used for the induction of ferroptosis [7, 8]. Many studies have presented the crucial function of ferroptosis in HCC development. It has been reported that the p62/Keap1/NRF2 signaling activation represses ferroptosis of HCC cells [9]. Quiescin sulfhydryl oxidase 1 contributes to sorafenib-stimulated ferroptosis by inactivating NRF2 activation and promoting EGFR endosomal trafficking in HCC [10].

Aspirin, a classical non-steroidal anti-inflammatory drug (NSAID), has been used in broad conditions including fever, pain, and inflammatory disease [11–13]. Recently, many epidemiological, clinical and experimental studies have shown that long-term use of aspirin can significantly reduce the incidence of cancer, delay the malignant process, impair the risk of tumor metastasis, and decrease cancer mortality [14–17]. Long-term follow-up study in several trials demonstrates that aspirin prevents the development of HCC, colorectal adenomas, breast and pancreatic cancers [18–22]. Our group has reported that aspirin inhibits the proliferation of hepatoma cells through controlling GLUT1-mediated glucose metabolism [23]. Although the benefit of aspirin for cancer patients has been widely appreciated, the mechanism behind remains largely unclear. It has been reported that nuclear factor κB (NF-κB) and Cox-2 can be served as targets of aspirin in many cancers [24–26]. Aspirin can inhibit the invasiveness of human cervical tumor cells through the

[1]Department of Gastrointestinal Cancer Biology, Tianjin Cancer Institute, Liver Cancer Center, Tianjin Medical University Cancer Institute and Hospital, National Clinical Research Center for Cancer, Tianjin 300060, China; [2]Tianjin's Clinical Research Center for Cancer, Tianjin 300060, China; [3]Department of Bone and Soft Tissue Tumors, Tianjin Medical University Cancer Institute and Hospital, National Clinical Research Center for Cancer, Tianjin 300060, China and [4]Department of Cancer Research, College of Life Sciences, Nankai University, Tianjin 300071, China
Correspondence: Guo-wen Wang (wangguowen@tmu.edu.cn) or Guang Yang (yangguang@tjmuch.com) or Xiao-dong Zhang (zhangxiaodong@tjmuch.com)
These authors contributed equally: Yu-fei Wang, Jin-yan Feng, Li-na Zhao, Man Zhao

Received: 9 January 2023 Accepted: 6 February 2023
Published online: 24 February 2023

suppression of matrix metalloproteinase 9 (MMP9) expression, while overexpression of NF-κB or c-Jun reverses the inhibitory effect of aspirin [27]. However, the target spectrum of aspirin in cancer cells and whether there are some other deep mechanisms remain to be investigated in HCC. The effect of aspirin on ferroptosis in HCC is poorly understood.

In this study, we are interested in the effect of aspirin on ferroptosis in HCC. Strikingly, we discovered that aspirin was capable of increasing ferroptosis. Interestingly, NF-κB p65 was able to activate the transcription of SLC7A11 through directly binding to the promoter of *SLC7A11*, resulting in the decrease of ferroptosis. Aspirin enhanced the ferroptosis by suppressing the NF-κB p65-regulated SLC7A11, and then decreased the growth of tumor. Thus, our findings provide new insights into the mechanism by which aspirin modulates ferroptosis in hepatocellular carcinoma.

MATERIALS AND METHODS

Cell lines, cell culture, and aspirin/PDTC treatment

Original cell lines were obtained from ATCC. Hepatoma cell lines such as HepG2, Huh7, osteosarcoma cell line (U2OS), human breast carcinoma cell line (MCF7), and human kidney epithelial (HEK) 293T cell line were cultured with Dulbecco's modified Eagle's medium (DMEM; Gibco, Grand Island, NY, USA) containing 10% fetal bovine serum (FBS, Gibco, NY, USA), 100 U/mL penicillin and 100 mg/mL streptomycin. All cell lines were cultured in 5% CO_2 and 37 °C conditions. For aspirin or PDTC treatment, the 1 M stock solution was prepared in DMSO. Cells were treated with 2 mM and/or 4 mM aspirin (Sigma–Aldrich, St. Louis, MO, USA) or 50 μM and/or 100 μM PDTC (MCE, NJ, USA) for 24 h.

Patient samples

Twenty-eight cases of HCC liver tumor tissues and their corresponding adjacent liver tissues were immediately obtained from Tianjin Medical University Cancer Institute and Hospital (Tianjin, China) after surgical resection for the extraction of mRNA. Clinicopathological information about the patients was obtained from patient records and was summarized in Supplementary Table S1. Written consents were obtained from each patient for research purposes after the operation. The study protocol was approved by the Institute Research Ethics Committee at Tianjin Medical University Cancer Institute and Hospital.

Plasmid construction and siRNAs

CDS regions of p65 (1656 bp) were cloned into pCMV-3Tag-1A via Nhe I/*Eco*R I (Promega, Madison, WI, USA). The 5′-flanking regions, −2000 bp to +200 bp (pGL3-p1), −2000 bp to −1665 bp (pGL3-p2), −1664 bp to −1053 bp (pGL3-p3), −1052 bp to −335 bp (pGL3-p4), −340 bp–0 (pGL3-p5), 0 to +200 bp (pGL3-p6) of *SLC7A11* promoter were synthesized from Sangon Biotech (Shanghai, China). All siRNAs were synthesized from Sangon Biotech (Shanghai, China). All primers and siRNA sequences were listed in Supplementary Table S2.

RNA extraction and RT-qPCR

Total RNA from hepatoma cells, clinical tissue samples and tumor tissue of BALB/c nude mice were isolated according to the TRIzol extraction method and reverse-transcription was performed using the HiFair III 1st Strand cDNA Synthesis SuperMix from YEASEN (Shanghai, China). RT-qPCRs were carried out using Hieff qPCR SYBR Green Master Mix from YEASEN. Fold changes of gene expression were calculated as $2^{-\Delta\Delta Ct}$. GAPDH was used as an internal control for normalization. All information of primer involved in the article is documented in Supplementary Table S2.

Western blot analysis

RIPA buffer was used to extract total protein lysates from cells or tissues. The protein lysates were subjected to SDS-PAGE, and then transferred to a nitrocellulose membrane. The membrane was blocked with 8% non-fat milk for 2 h and incubated with first antibody for 1 h at room temperature. After incubation with the secondary antibody for 1 h at 37 °C, the membrane was visualized by ECL Western Blotting Detection Kit from GE Healthcare (Waukesha, WI, USA). All the antibodies were listed in Supplementary Table S3.

Chromatin immunoprecipitation (ChIP)

ChIP assays were performed in HepG2 and Huh7 cells transfected with p65-pCMV-3Tag-1A or pCMV-3Tag-1A vector according to the manufacturer's protocol (Epigentek Group Inc, Brooklyn, NY, USA) as reported previously [28]. All primers are listed in Supplementary Table S2. All experiments were performed at least three times.

RNA-seq analysis

Total RNA was extracted from HepG2 cells treated with aspirin or DMSO, and subjected to RNA-seq analysis performed by Shanghai Majorbio Bio-pharm Technology Co.,Ltd. The data were analyzed on the free online platform of Majorbio Cloud Platform (https://www.majorbio.com/).

Luciferase reporter gene assays

Luciferase reporter gene assays were performed using the Dual-Luciferase Reporter Assays System (Promega, Madison, WI, USA) according to the manufacturer's instructions. Cells were transferred into 24-well plates at 3×10^4 cells/well. After 12 h, the cells were transiently co-transfected with 0.1 μg/well of pRL-TK plasmid (Promega, USA) containing the Renilla luciferase gene used for internal normalization and pGL3-SLC7A11 plasmid. The luciferase activities were measured as previously described [29]. All experiments were performed at least three times.

Cell viability and proliferation assays

The protocol was described previously [29]. CCK-8 assays were performed to examine the cell viability. Hepatoma cells were seeded into 96-well plates (2000 cells/well) for 12 h and treated with DMSO, erastin, ferrostatin-1, aspirin, PDTC or transfected with p65-pCMV-3Tag-1A and sip65 for 24 h. *OD* values of cells were measured using a microplate reader at 490 nm. For cell proliferation assays, hepatoma cells were seeded into 96-well plates (2000 cells/well) for 12 h before transfection. CCK-8 assays were used to assess cell proliferation every 24 h from the first day until 72 h after transfection. For colony formation analysis, 1000 viable cells were plated in 6-well plates after 48 h transfection, and cultured in complete medium for 2 weeks. Colonies were fixed with methanol and stained with 0.1% crystal violet.

In vivo tumorigenicity assays

BALB/c athymic nude mice were obtained from Beijing HFK Bioscience Co.,Ltd. HepG2 cells were transfected with pCMV-3Tag-1A vector (control), p65-pCMV-3Tag-1A by using Lipofectamine RNAiMAX (Invitrogen, Carlsbad, CA, USA). Forty-eight hours after transfection, HepG2 cells were harvested and suspended at 1×10^7 cells/mL in 0.2 mL of PBS in separate sets of mice, and then injected into the subcutaneous region of 6-week-old male BALB/c athymic nude mice, six mice per group. A week later, mice co-treated with aspirin and p65 were daily treated with intragastric gavage with aspirin (suspended in physiological saline, 75 mg/kg). Mice in co-treatment with aspirin, p65 and erastin group were daily treated with both intragastric gavage with aspirin (suspended in physiological saline, 75 mg/kg) and intraperitoneal (i.p.) erastin (20 mg/kg) with solution (10% DMSO + 40% PEG300 + 50% saline). After 5 days of the injection, the

tumor growth was measured every 5 days. Blind measurements were carried out to avoid unconscious biases. After 30 days, mice were euthanized and tumors were sectioned. The levels of intracellular GSH/GSSG were determined by using GSH/GSSG assays kit, the expression of p65 and SLC7A11 was measured by RT-qPCR or Western blot analysis. The paraffin-embedded slides were made. Tumor volume was monitored by measuring the length (L) and width (W) with calipers and calculated with the formula $(L \times W^2) \times 0.5$. The study was authorized by the Ethics Committee of Tianjin Medical University and performed in accordance with the Declaration of Helsinki. All the animal experiments were approved by Tianjin Medical University Animal Care and Use Committee.

Iron assays

Intracellular ferrous iron (Fe^{2+}) levels were determined by using the iron assays kit (ab83366) purchased from Abcam (Cambridge, UK) according to the manufacturer's instructions. Cells were seeded onto 10-cm cell dish (5×10^6 cells/dish) and treated with DMSO, erastin, aspirin and/or PDTC for 24 h. Cells were collected and washed in ice-cold PBS and homogenized in 5 × volumes of iron assays buffer on ice, then centrifuged for 10 min, 16,000 × g at 4 °C to remove insoluble material. The supernatant was collected and assays buffer was added to each sample, mixed and incubated for 30 min at room temperature. An 100 µL of iron probe was added, mixed and incubated at 37 °C for 60 min at dark condition. The absorbance was measured at 593 nm using a microplate reader.

Lipid ROS assays

Lipid ROS levels were analyzed by flow cytometry using BODIPY-C11 dye [30]. Cells were seeded at 2.5×10^5 per well in six-well plates. Twelve hours later, cells were treated with DMSO, erastin, aspirin and/or PDTC for 24 h. The culture medium was replaced with 2 mL medium containing 10 µM of BODIPY-C11 (Thermo Fisher, Cat# D3861, USA) and incubated at 37 °C for 1 h. Cells were harvested and washed twice with PBS to remove excess BODIPY-C11. The cells were re-suspended in 500 µL of PBS and filtered through cell strainer (0.4 µm nylon mesh) and subjected to the flow cytometry analysis to examine the amount of lipid ROS within cells. The fluorescence intensities of cells per sample were examined by flow cytometry using the BD FACS Aria cytometer (BD Biosciences, USA). A minimum of 10,000 cells was analyzed per condition.

Malondialdehyde (MDA) assays

Lipid peroxidation assay kit (Abcam, ab118970, Cambs, UK) was used to assess the relative MDA concentration in cell lysates according to the manufacturer's instructions. Cells were seeded in 10 cm plate with 5×10^6 cells/plate overnight. The cells were treated with DMSO, erastin, aspirin or PDTC for 24 h. Cells were washed with ice-cold PBS and homogenized on ice in 300 µL of the MDA lysis buffer with 3 µL BHT, then centrifuged at 13,000 × g, for 10 min to remove insoluble material. The supernatant from each homogenized sample (200 µL) was placed into a microcentrifuge tube. TBA solution of 600 µL was added into each vial. The samples were incubated at 95 °C for 60 min. The samples were cooled to room temperature in an ice bath for 10 min. The reaction mixture of 200 mL was transferred into a 96-well plate and the absorbance was measured at 532 nm using a microplate reader.

GSH/GSSH assays

The relative glutathione (GSH) concentration in cells or tissues was examined by using the glutathione assay kit (Sigma, CS0260, MO, USA) according to the manufacturer's instructions. Cells were seeded into 10 cm plate with 5×10^6 cells/plate overnight and treated with DMSO, erastin, aspirin or PDTC for 24 h. Cells were washed with ice cold PBS and lysed in 1% lysis buffer (25 mM Tris at pH 7.5, 300 mM NaCl, 1 mM EDTA, 0.5% NP-40) supplemented with a phosphatase inhibitor mix (Pierce) and a complete protease inhibitor cocktail (Roche). After sonication (Thermo Model 120, amplitude 15%, push-on time 5 s, process time 10 s and push-off time 1 s), cell lysates were centrifuged at 13,000 r/min at 4 °C for 10 min, and cleared lysate was used to determine the amount of GSH in the sample. GSH assay mixture (50 µL) was added into each sample well, incubated at room temperature for 60 min, and protected from light. GSH was measured by using a microplate reader at 412 nm. The relative GSSG concentration in cells or tissues was assessed using a kit from Cayman (#703002, USA) according to the manufacturer's instructions. Cells were seeded onto 10 cm plate with 5×10^6 cells/plate and treated with DMSO, erastin, aspirin or PDTC for 24 h. Cells were collected in 15 mL tubes and washed with ice cold PBS three times. Cells were homogenized in 2 mL of cold 50 mM MES buffer, and then centrifuged at 10,000 × g, for 15 min at 4 °C to remove insoluble material. The quantification of GSSG, exclusive of GSH, was accomplished by derivatizing GSH with 2-vinylpyridine (Sigma, 13229-2, MO, USA). The supernatant was collected and 10 µL of 2-vinylpyridine solution was added (1 M in ethanol) for per mL of sample. The sample was mixed well and incubated for 60 min at room temperature to block the thiol group of the GSH already present. NADPH (2 mg/mL) in water and 5 µL of 2 U/mL glutathione reductase was added to reduce GSSG. Sample (50 µL) was added into each well of 96-well plate and mixed with 150 µL assay cocktail mixture. The plate was incubated in the dark on a shaker for 30 min and the absorbance was measured at 412 nm by using a microplate reader.

Immunohistochemical (IHC) staining

Tumor tissues from nude mice were fixed and embedded in paraffin after the mice were sacrificed. Immunohistochemical analysis was performed as described previously [31]. Anti-HNE primary antibodies were used in Supplementary Table S3.

Statistical analysis

Each experiment was repeated at least three times unless otherwise indicated. All analysis and graphs were generated with GraphPad Prism 6. Statistical significance was assessed by comparing mean values (±SD) using a student's t-test for independent groups and was expressed for $^*P < 0.05$; $^{**}P < 0.01$; $^{***}P < 0.001$.

RESULTS

Aspirin is involved in ferroptosis in HCC cells

Although it has been reported that aspirin depresses cell proliferation in HCC [32–34], we still wondered the target spectrum of aspirin and whether there are some other deep mechanisms in HCC. We performed RNA-seq analysis with HepG2 cells treated with aspirin. The profiling of RNA-seq analysis showed that aspirin regulated the expression of 1499 genes, including 1099 down-regulation genes and 400 up-regulation ones ($|\log2$ fold change$| \geq 1.5$, P adjust <0.05, Fig. 1a and Supplementary Fig. S1). Moreover, the GO analysis indicated that aspirin modulated cellular process, biological regulation, metabolic process, catalytic activity and etc. (Fig. 1b). KEGG pathway analysis revealed that aspirin treatment led to several biological aspects including signal transduction, immune disease, cell growth and cell death, cellular community, replication and repair, amino acid metabolism and lipid metabolism (Fig. 1c), suggesting that aspirin has widespread effects on liver cancer cells.

As ferroptosis is a form of programming cell death, involving cancer development and answering the drug treatment [35–38], we calculated and drew custom Venn diagrams with the RNA-seq data and ferroptosis-related data from FerrDb (http://www.zhounan.org/ferrdb/current/). As shown in Fig. 1d, aspirin

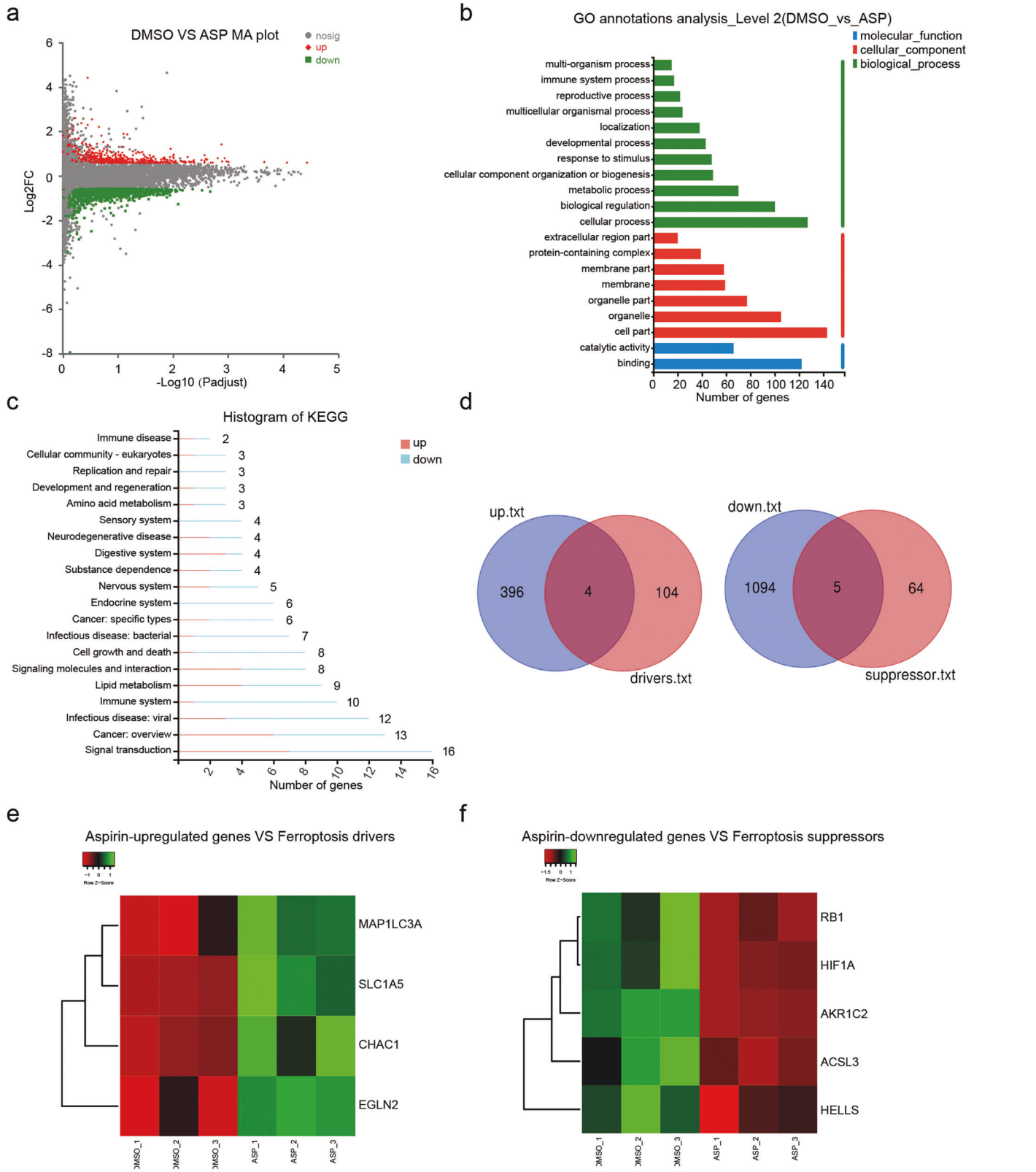

Fig. 1 Aspirin is involved in ferroptosis in HCC cells. a MA plot indicating the differently expressed genes identified by RNA-seq analysis in HepG2 cells treated with 4 mM aspirin (|log2 fold change| ≥1.5, *P* adjust <0.05). **b** GO functional enrichment analysis was performed to analyze the functions of aspirin-regulated genes. **c** KEGG enrichment analysis was performed to analyze the aspirin-regulated pathways. **d** Custom Venn diagrams were generated by using the RNA-seq data and ferroptosis-related data from FerrDb. **e**, **f** Cluster analysis indicated the ferroptosis-related genes were differentially regulated by aspirin according to the RNA-seq data.

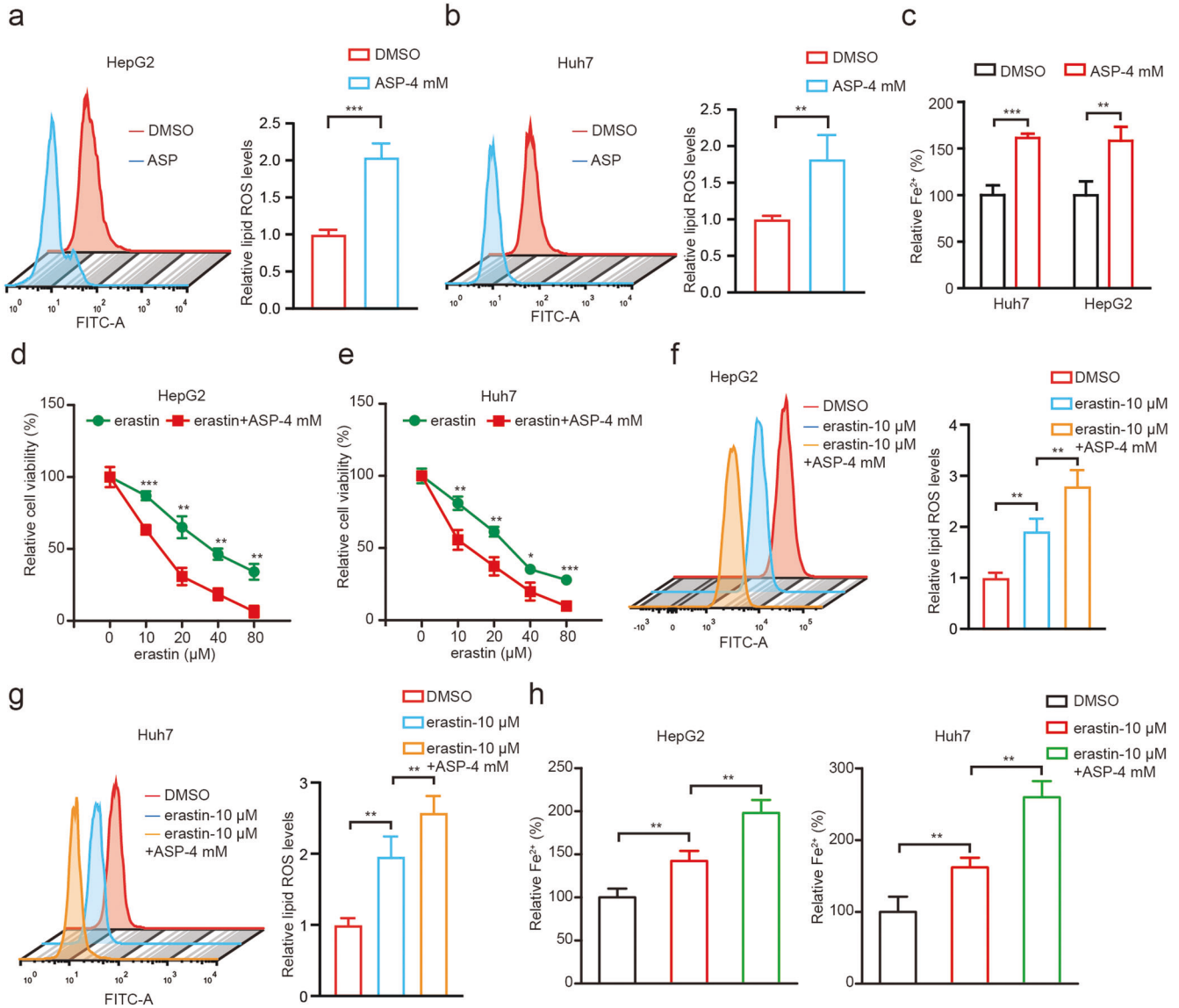

Fig. 2 Aspirin triggers ferroptosis in HCC cells. a, **b** Lipid ROS levels were assessed by flow cytometric analysis in HepG2 and Huh7 cells treated with 4 mM aspirin. **c** Accumulation of Fe^{2+} was measured by an iron assay in HepG2 and Huh7 cells treated with 4 mM aspirin. **d**, **e** The cell viability was determined by CCK-8 assays in HepG2 and Huh7 cells treated with 4 mM aspirin and different erastin concentrations 0, 10, 20, 40, 80 μM, respectively. **f**, **g** Lipid ROS levels were assessed by flow cytometric analysis in HepG2 and Huh7 cells treated with 10 μM and/or 4 mM aspirin. **h** Accumulation of Fe^{2+} was explored by an iron assay in HepG2 and Huh7 cells treated with 10 μM and/or 4 mM aspirin. Data are shown as mean ± SD and representative of three independent experiments. $^{*}P < 0.05$; $^{**}P < 0.01$; $^{***}P < 0.001$.

up-regulated 4 of ferroptosis-related drivers and down-regulated 5 of ferroptosis-related suppressors. Next, we demonstrated the cluster analysis for those induced ferroptosis-related factors (Fig. 1e, f). Thus, we conclude that aspirin treatment is potentially relevant to the incidence of ferroptosis in HCC.

Aspirin triggers ferroptosis in HCC cells

To further evaluate the effect of aspirin on ferroptosis in HCC, we adopted erastin, a classical small-molecule inducers of ferroptosis [39]. Interestingly, we observed that the erastin treatment significantly inhibited liver cancer cell viability, which was sharply counteracted by the ferroptosis inhibitor ferrostatin-1, indicating that erastin-induced ferroptosis can affect the growth of liver cancer cells (Supplementary Fig. S2a, b). To test whether aspirin can modulate ferroptosis in liver cancer cells, we evaluated the levels of ferrous iron (Fe^{2+}) and lipid ROS that are inducers and indicators for ferroptosis [39]. Interestingly, we clearly found that aspirin treatment could remarkably increase the levels of lipid ROS (Fig. 2a, b) and Fe^{2+} (Fig. 2c) in HepG2 and Huh7 cells. Accordingly, we next treated the cells with both erastin and aspirin, where aspirin further enhanced cell death induced by erastin (Fig. 2d, e), implying that aspirin might inhibit cell viability through modulating ferroptosis in cells. Moreover, we found that the levels of erastin-induced lipid ROS production and Fe^{2+} accumulation were higher in hepatoma cells treated with aspirin relative to single treatment (Fig. 2f–h). Thereby, we conclude that aspirin can induce the ferroptosis in hepatoma cells in a model (Supplementary Fig. S2c).

The NF-κB p65 restricts ferroptosis in liver cancer cells

It has been reported that NF-κB is frequently involved in the aspirin-mediated modulation of cellular metabolism and proliferation [40–42]. Accordingly, we explored the responded effects including cell viability, Fe^{2+} and lipid ROS to erastin and PDTC, an

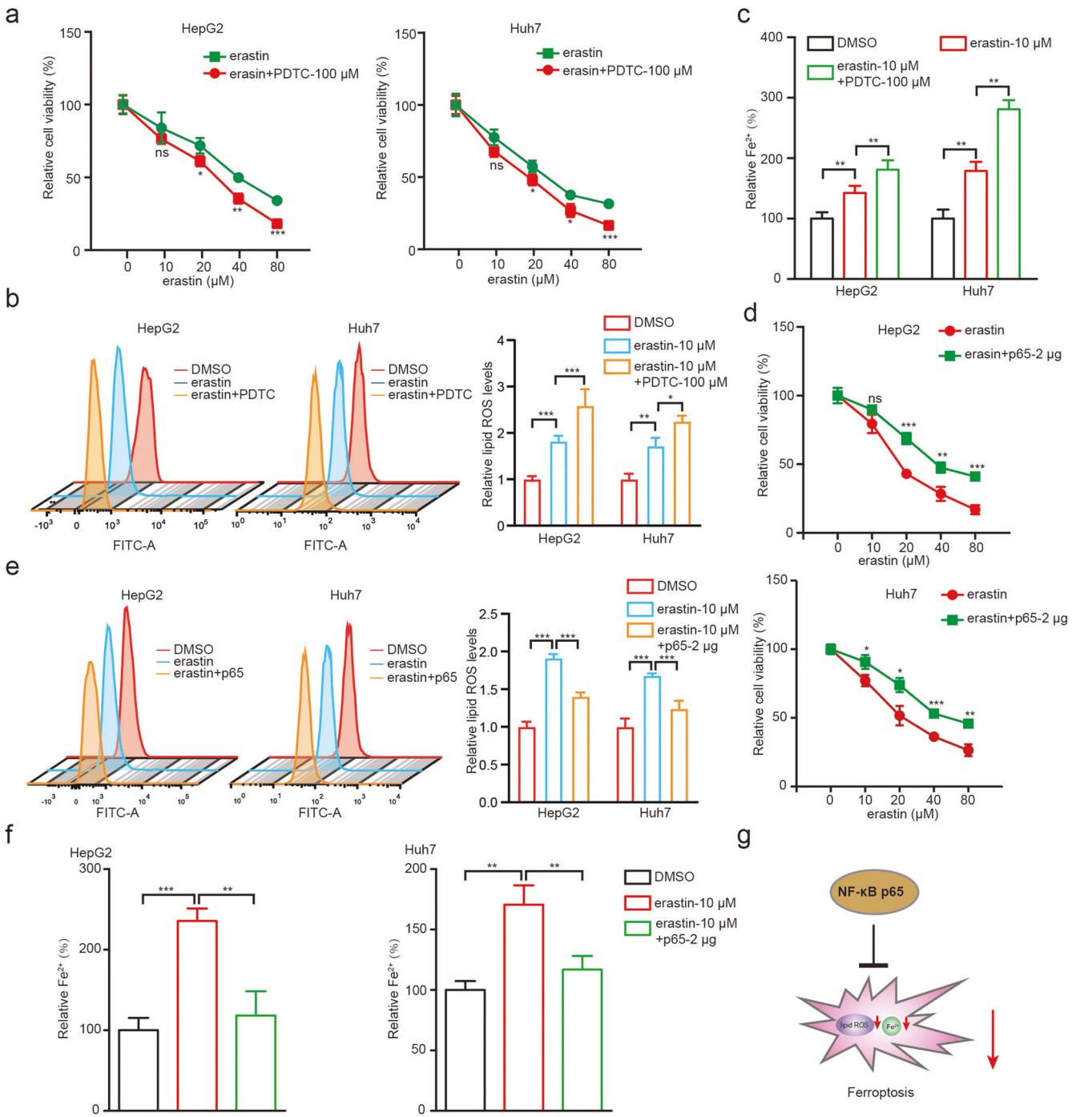

Fig. 3 The NF-κB p65 restricts ferroptosis in liver cancer cells. a The cell viability was examined by CCK-8 assays in HepG2 and Huh7 cells treated with 100 μM PDTC and different erastin concentrations 0, 10, 20, 40, 80 μM, respectively. **b** Lipid ROS levels were assessed by flow cytometric analysis in HepG2 and Huh7 cells treated with 10 μM erastin and/or 100 μM PDTC. **c** Accumulation of Fe^{2+} was measured by an iron assay in HepG2 and Huh7 cells treated with 10 μM erastin and/or 100 μM PDTC. **d** The cell viability was examined by CCK-8 assays in HepG2 and Huh7 cells treated with 2 μg p65 and different erastin concentrations 0, 10, 20, 40, 80 μM, respectively. **e** Lipid ROS levels were assessed by flow cytometric analysis in HepG2 and Huh7 cells treated with 10 μM erastin and/or 2 μg p65. **f** Accumulation of Fe^{2+} was measured by an iron assay in HepG2 and Huh7 cells treated with 10 μM erastin and/or 2 μg p65. **g** A model of NF-κB p65 restricts ferroptosis in liver cancer cells. Data are shown as mean ± SD and representative of three independent experiments. $^{*}P < 0.05$; $^{**}P < 0.01$; $^{***}P < 0.001$; ns no significance.

inhibitor of NF-κB in HepG2 and Huh7 cell lines. Interestingly, we identified that PDTC promoted erastin-induced cell death (Fig. 3a), as well as further increased the levels of erastin-induced lipid ROS (Fig. 3b) and Fe^{2+} (Fig. 3c) in HepG2 and Huh7 cells, suggesting that NF-κB pathway participates in the process of ferroptosis in hepatoma cells.

Given that p65 protein functioned as a key subunit of NF-κB plays critical role in NF-κB-related pathways [43–45], we then investigated whether p65 could modulate erastin-induced ferroptosis. For the first, we assessed the efficacy of overexpression and knockdown of p65 in HCC cells (Supplementary Fig. S3a, b). As shown in Supplementary Fig. S3b, we found that sip65#2 significantly

down-regulated the levels of p65. Using the CCK-8 assays, we found that overexpression of p65 attenuated the erastin-induced cell death in HepG2 and Huh7 cell lines (Fig. 3d). On the contrary, knockdown of p65 could markedly enhance the erastin-induced cell death in cells (Supplementary Fig. S3c). Similarly, erastin-induced accumulation of lipid ROS (Fig. 3e and Supplementary Fig. S3d) and Fe^{2+} (Fig. 3f and Supplementary Fig. S3e) were significantly reversed by overexpression of p65 and enhanced by sip65 in cells, suggesting that p65 as an NF-κB subunit inhibits ferroptosis. Taken together, we conclude that NF-κB p65 restricts ferroptosis in liver cancer cells in a model (Fig. 3g).

Aspirin induces ferroptosis through NF-κB p65 in HCC cells

Since NF-κB p65 could modulate erastin-induced ferroptosis, we then validated the aspirin-NF-κB p65-ferroptosis axis in HCC cells. As shown in Fig. 4a, cells with PDTC treatment displayed lower viability on the basis of aspirin. Nevertheless, overexpression of p65 could partially rescue the aspirin-triggered decrease of cell viability (Fig. 4b). Accordingly, we examined the levels of lipid ROS and Fe^{2+} in HCC cells treated with different regiments. As expected, we found that aspirin significantly stimulated the accumulation of lipid ROS and Fe^{2+}, which could be markedly reversed by overexpression of p65, and further be enhanced by treatment with PDTC (Fig. 4c, d). As MDA is one of the most important end-products of ferroptosis [8], we explored whether aspirin or NF-κB regulated MDA accumulation in hepatoma cells. As shown in Fig. 4e, aspirin increased the erastin-induced MDA levels, which could be further enhanced by PDTC treatment; however, the elevated levels of MDA induced by aspirin were significantly suppressed by the overexpression of NF-κB p65, suggesting that aspirin induces ferroptosis through NF-κB p65 in hepatoma cells.

To assess whether aspirin-induced ferroptosis was universally functioned in cancers, we explored the effect in MCF7 (human breast carcinoma cell line) and U2OS (osteosarcoma cell line) cells. As depicted in Supplementary Fig. S4a, we found that aspirin significantly enhanced the erastin-induced cell viability inhibition in both MCF7 and U2OS cells, and PDTC increased that in this event. On the contrary, overexpression of p65 blocked aspirin-medicated cell viability decrease (Supplementary Fig. S4b). Accordingly, we observed that aspirin significantly elevated the levels of lipid ROS, Fe^{2+} and MDA, which could be further enhanced by treatment with PDTC or blocked by overexpression of p65 in MCF7 and U2OS cells (Supplementary Fig. S4c–e), suggesting that aspirin regulates ferroptosis through NF-κB p65 in human breast cancer cells and osteosarcoma cells. Thus, we conclude that aspirin induced ferroptosis through NF-κB p65 in cancer cells in a model (Fig. 4f).

Aspirin induces ferroptosis through inhibiting NF-κB p65-activated SLC7A11 transcription in cancer cells

To clarify the mechanism by which aspirin-targeted NF-κB p65 modulates ferroptosis, some known ferroptosis-related genes including VDAC2, ALOX15, SLC1A5, ALOX5, ACSL4, GPX4, and SLC7A11 were tested. Remarkably, we identified that overexpression of p65 sharply up-regulated the mRNA levels of SLC7A11, especially among the above 7 genes in HepG2 and Huh7 cell lines (Fig. 5a and Supplementary Fig. S5a). Oppositely, knockdown of p65 most particularly inhibited the mRNA expression of SLC7A11 in cells (Fig. 5b and Supplementary Fig. S5b), indicating that aspirin/NF-κB p65 axis might modulate the ferroptosis through regulating the expression of SLC7A11. To better understand the effect of p65 and SLC7A11 on HCC progress, we assessed that HCC patients with high expression of SLC7A11 and p65 presented lower survival rate by the Gene Expression Profiling Interactive analysis data ($n = 182$, $P < 0.05$, Fig. 5c and Supplementary Fig. S5c). In addition, we demonstrated the correlation between SLC7A11 and p65 expression in 28 clinical liver cancer tissues. RT-qPCR assays showed that the mRNA levels of p65 were positively associated with those of SLC7A11 in the tissues (Fig. 5d). Moreover, we confirmed that SLC7A11 was up-regulated by p65, but down-regulated by sip65 in a dose-dependent manner in HepG2 and Huh7 cell lines (Fig. 5e and Supplementary Fig. S5d). Correspondingly, we further observed that PDTC treatment remarkably down-regulated the expression of SLC7A11 in a dose-dependent manner in cells (Fig. 5f), suggesting that NF-κB p65 can sharply up-regulate the expression of SLC7A11.

Next, we try to clarify the mechanism by which p65 up-regulated SLC7A11. As p65 functioned as a transcription factor, we proposed that SLC7A11 might be regulated by p65. Accordingly, we constructed the full length plasmid of *SLC7A11* promoter, termed pGL3-p1. As expected, the luciferase activity of pGL3-p1 was remarkably increased by p65 in cells in a dose-dependent manner (Fig. 5g). Then, we identified the core region of *SLC7A11* promoter. Various lengths of the *SLC7A11* 5′flanking regions, including −2000 bp to −1665 bp (pGL3-p2), −1664 bp to −1053 bp (pGL3-p3), −1053 bp to −335 bp (pGL3-p4), −340 bp–0 (pGL3-p5), and 0 to +200 bp (pGL3-p6) were synthesized and transiently transfected into the HepG2 and Huh7 cells, respectively. The luciferase reporter gene assays indicated that the fragment of pGL3-p5 exhibited the maximum luciferase activities than the other truncates (Fig. 5h), indicating that the region of −340 bp–0 may be the core region of *SLC7A11* promoter regulated by p65. In addition, ChIP-qPCR assays displayed that p65 could be richened on the core region of *SLC7A11* promoter in hepatoma cells (Fig. 5i), suggesting that p65 up-regulates the expression of SLC7A11 through binding on the core promoter region of *SLC7A11* and activating the transcription of SLC7A11. Next, we found that aspirin or PDTC could down-regulate the transcription activities of SLC7A11, which could be strongly rescued by overexpression of p65 in the cells (Fig. 5j and Supplementary Fig. S5e). Moreover, aspirin-suppressed SLC7A11 could be rescued by overexpression of p65, which was consistent with the levels of GSH/GSSG, the SLC7A11 regulated substance, also an index of ferroptosis (Fig. 5k–m and Supplementary Fig. S5f). Accordingly, overexpression of SLC7A11 blocked the aspirin-mediated ferroptosis significantly (Fig. 5n and Supplementary Fig. S5g), suggesting that aspirin induces ferroptosis by modulating SLC7A11. To assess whether aspirin-induced ferroptosis functioned in other cancers, we explored that in MCF7 and U2OS cells. As depicted in Supplementary Fig. S5h–j, we found that aspirin/NF-κB p65-ferroptosis axis also worked in other types of cancers. Thus, we conclude that aspirin induces ferroptosis through inhibiting NF-κB p65-activated SLC7A11 transcription in cancer cells.

Aspirin confers p65-mediated ferroptosis to inhibit the growth of cancers in vitro and in vivo

Accordingly, we concerned whether aspirin could inhibit the proliferation of hepatoma cells through modulating p65-inhibited ferroptosis. We first analyzed the relationship between p65/SLC7A11 and HCC by using TCGA database. We observed that both p65 and SLC7A11 were up-regulated in HCC tumor tissues relative to their adjacent tissues and the expression of both was increased by tumor grade (Supplementary Fig. S6a–d). Next, CCK-8 and colony formation assays revealed that aspirin inhibited the cell proliferation, which could be reversed by overexpression of p65, and be enhanced by the co-treatment of erastin (Fig. 6a, b), suggesting that aspirin suppresses the proliferation of hepatoma cells through p65-mediated inhibition of ferroptosis in vitro. Accordingly, we confirmed that in MCF7 and U2OS cell lines (Supplementary Fig. S6e–g). To better understand the role of aspirin/p65 in promotion of hepatocarcinogenesis in vivo, we subcutaneously injected the pretreated cells into 4-week-old BALB/c athymic nude mice. Strikingly, we demonstrated that the

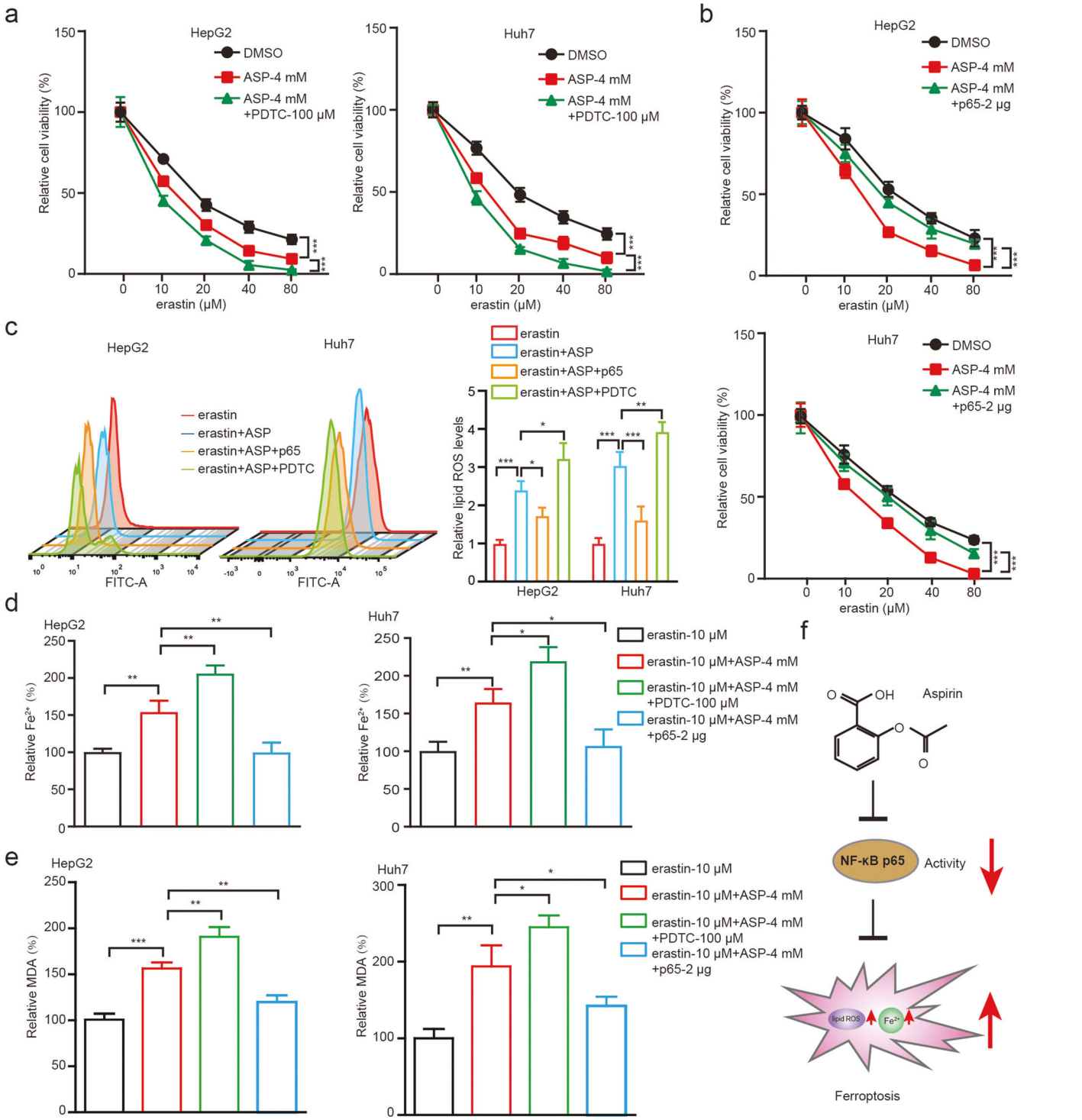

Fig. 4 Aspirin induces ferroptosis through NF-κB p65 in HCC cells. a The cell viability was measured by CCK-8 assays in HepG2 and Huh7 cells treated with 4 mM aspirin and/or 100 μM PDTC and different erastin concentrations 0, 10, 20, 40, 80 μM, respectively. **b** The cell viability was measured by CCK-8 assays in HepG2 and Huh7 cells treated with 4 mM aspirin and/or 2 μg p65 and different erastin concentrations 0, 10, 20, 40, 80 μM, respectively. **c** Lipid ROS levels were assessed by flow cytometric analysis in HepG2 and Huh7 cells treated with 10 μM erastin, 10 μM erastin+4 mM aspirin, 10 μM erastin+4 mM aspirin+2 μg p65 and 10 μM erastin+ 4 mM aspirin+100 μM PDTC, respectively. **d** Accumulation of Fe^{2+} was explored by an iron assay in HepG2 and Huh7 cells treated with 10 μM erastin, 10 μM erastin+4 mM aspirin, 10 μM erastin+ 4 mM aspirin+2 μg p65 and 10 μM erastin+4 mM aspirin+100 μM PDTC, respectively. **e** The levels of MDA were analyzed by an MDA assay in HepG2 and Huh7 cells treated with 10 μM erastin, 10 μM erastin+4 mM aspirin, 10 μM erastin+4 mM aspirin+2 μg p65 and 10 μM erastin+4 mM aspirin+100 μM PDTC, respectively. **f** A model of aspirin suppresses ferroptosis through NF-κB p65 in cancer cells. Data are shown as mean ± SD and representative of three independent experiments. *$P < 0.05$; **$P < 0.01$; ***$P < 0.001$; ns no significance.

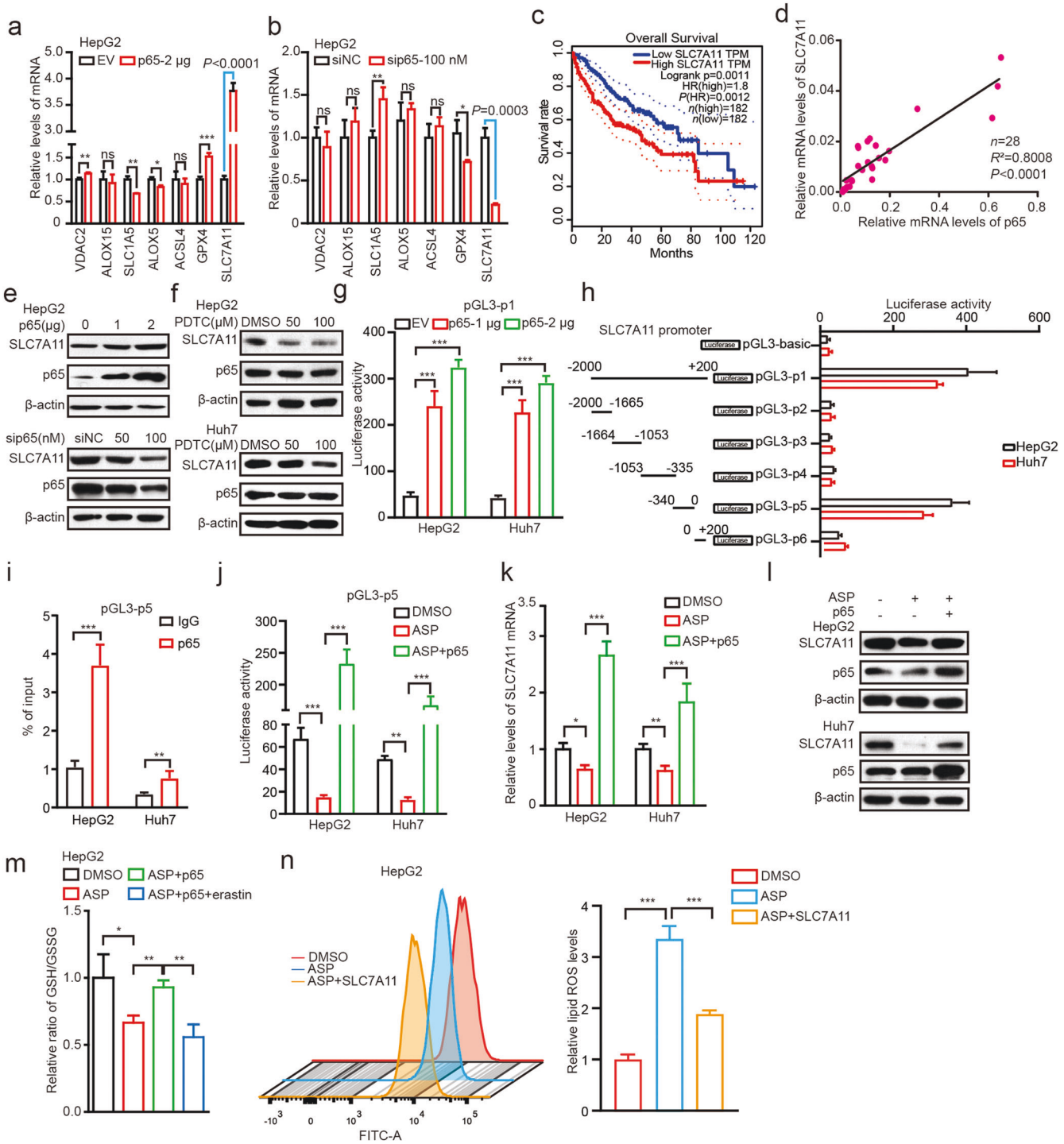

Fig. 5 Aspirin induces ferroptosis through inhibiting NF-κB p65-activated SLC7A11 transcription in cancer cells. a, **b** The mRNA levels of VDAC2, ALOX15, SLC1A5, ALOX5, ACSL4, GPX4 and SLC7A11 were measured by RT–qPCR in HepG2 cells transfected with 2 μg p65 or 100 nM sip65. **c** The survival curves of HCC patients with low or high SLC7A11 expression by using TCGA data. **d** The relevance between p65 and SLC7A11 mRNA in HCC clinical tumor tissues was explored by RT-qPCR. **e** The protein levels of SLC7A11 and p65 in HepG2 cells transfected with p65 or sip65 were analyzed by Western blot analysis. **f** The protein levels of SLC7A11 and p65 in HepG2 and Huh7 cells treated with PDTC were analyzed by Western blot analysis. **g** The transcriptional activity of the *SLC7A11* promoter was measured by dual-luciferase reporter assays in HepG2 and Huh7 cells transfected with p65. **h** The transcriptional activity of the different regions of *SLC7A11* promoter was measured by a dual-luciferase reporter assay in HepG2 and Huh7 cells transfected with 2 μg p65. **i** The enrichment of p65 on the *SLC7A11* region of −340 bp– 0 was examined by ChIP-qPCR assay in HepG2 and Huh7 cells transfected with 2 μg p65. **j** The transcriptional activity of the SLC7A11 core promoter region was analyzed by dual-luciferase reporter assays in HepG2 and Huh7 cells transfected with DMSO, 4 mM aspirin and 4 mM aspirin+2 μg p65. **k**, **l** The mRNA and protein levels of SLC7A11 were measured by RT-qPCR and Western blot analysis in HepG2 and Huh7 cells treated with 4 mM aspirin and/or 2 μg p65. **m** The ratio of GSH/GSSG was analyzed by GSH and GSSG assays in HepG2 cells treated with DMSO, 4 mM aspirin, 4 mM aspirin+2 μg p65, 4 mM aspirin+2 μg p65+10 μM erastin, respectively. **n** Lipid ROS levels were assessed by flow cytometric analysis in HepG2 cells treated with 4 mM aspirin and 4 mM aspirin+2 μg SLC7A11. Data are shown as mean ± SD and representative of three independent experiments. *$P < 0.05$; **$P < 0.01$; ***$P < 0.001$; ns no significance.

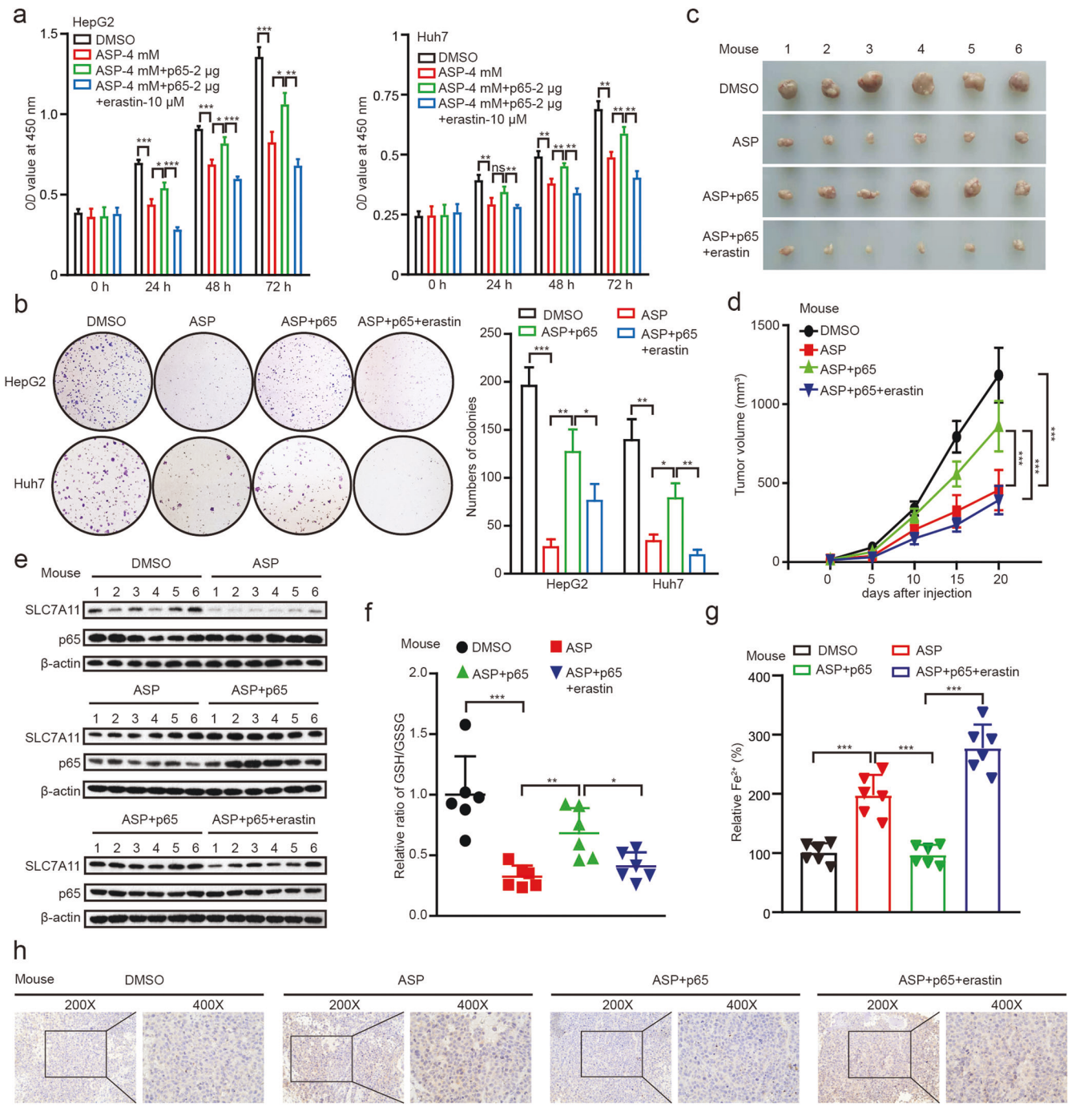

Fig. 6 Aspirin confers p65-mediated ferroptosis to inhibit the growth of cancers in vitro and in vivo. a, **b** The proliferation was measured by CCK-8 and colony formation assays in HepG2 and Huh7 cells treated with DMSO, 4 mM aspirin, 4 mM aspirin+2 μg p65, 4 mM aspirin+2 μg p65+10 μM erastin, respectively. **c**, **d** The effects of DMSO, 75 mg/kg aspirin, 75 mg/kg aspirin+p65 and 75 mg/kg aspirin+p65+20 mg/kg erastin on the growth of hepatoma cells were analyzed in a xenograft mouse model. Representative tumor images (**c**) and tumor volume data (**d**) are shown. **e** The protein levels of SLC7A11 and p65 in tumor tissues were examined by Western blot analysis. **f**, **g** The ratio of GSH/GSSG and the levels of Fe^{2+} were analyzed by GSH/GSSG and Fe^{2+} assays in tumor tissues from mice. **h** Paraffin sections of tumor samples were used for IHC staining with antibodies against 4-HNE. Magnification, 200× and 400×. Data are shown as mean ± SD and representative of three independent experiments. *$P < 0.05$; **$P < 0.01$; ***$P < 0.001$; ns no significance.

treatment with aspirin sharply suppressed the growth of liver cancer in mice. We observed that the tumor volume and tumor weight were remarkably decreased by treatment with aspirin, which could be reversed by overexpression of p65, while be attenuated by co-treatment with erastin (Fig. 6c, d and Supplementary Fig. S6h). Western blot analysis validated that the expression levels of SLC7A11 were decreased in the group of mice treated with aspirin, which could be rescued by overexpression of p65 (Fig. 6e). Moreover, we determined the levels of GSH/GSSG, Fe^{2+} and lipid peroxide 4-hydroxynonenal (4-HNE) for ferroptosis in the mouse tumor samples. The results revealed that p65 could block the aspirin-mediated ferroptosis, and erastin could eliminate the p65-induced suppression of ferroptosis (Fig. 6f–h). Therefore, we conclude that aspirin increases

ferroptosis by targeting p65, which contributes to the inhibition of cancer growth.

DISCUSSION

A growing number of studies have suggested that aspirin has anticancer effects. Recently, Lee and colleagues have reported that aspirin prevents the development of HCC [46]. Our group previously reported that aspirin suppressed the development of hepatoma cells through modulating the lipid metabolism and glucose metabolism [23, 47]. However, whether aspirin could regulate ferroptosis in suppression of liver cancer is poorly understood. In this study, we investigated the significance of aspirin in the modulation of ferroptosis.

Firstly, we performed RNA-seq to explore the function of aspirin in hepatoma cells, especially searching for the effect of aspirin on ferroptosis. Surprisingly, the RNA-seq analysis revealed that aspirin is positive associated with ferroptosis. Given that ferroptosis is iron-dependent cell death characterized by intracellular ROS accumulation, we adopted the assays to test the cell viability and the levels of ROS and ferrous iron [48]. Notably, we found that aspirin could stimulate the levels of lipid ROS and Fe^{2+}, and suppress the proliferation of liver cancer cells. It suggests that aspirin may modulate ferroptosis in HCC. To better understand the significance of aspirin in modulating ferroptosis, we firstly adopted erastin, which was a ferroptosis inducer that down-regulated the GSH level by inhibiting system Xc^- [49, 50]. Strikingly, aspirin remarkably enhanced the effect of erastin on cell viability, the levels of ROS and Fe^{2+} in hepatoma cells. Therefore, our finding provides evidence that aspirin modulates ferroptosis in liver cancer.

Next, we try to identify the mechanism by which aspirin regulates ferroptosis. It has been reported that NF-κB was frequently involved in aspirin-mediated modulation of cellular metabolism and proliferation [40–42]. Interestingly, we identified that PDTC promoted erastin-induced cell death, as well as further increased the levels of erastin-induced lipid ROS and Fe^{2+} in hepatoma cells. It suggests that NF-κB pathway participates in the process of ferroptosis in HCC cells. The most abundant form of NF-κB is the p65:p50 heterodimer. Disproportionate increase in activated p65 and subsequent transactivation of effector molecules is integral to the pathogenesis of many chronic diseases [51]. Hence, the NF-κB p65 is a potential target for drug development. Strikingly, erastin-induced accumulation of lipid ROS and Fe^{2+} was significantly up-regulated by sip65 and reversed by overexpression of p65 in HCC cells. It suggests that p65 as a NF-κB subunit modulates ferroptosis in HCC cells. It has been reported that PDTC as a metal ion chelator can chelate iron ions [52], which may affect ferroptosis. Comparing the effects of PDTC on ferroptosis with those of sip65 on ferroptosis in Fig. 3b, c and Supplementary Fig. S3d, e, we found that the former was stronger than latter. It implies that PDTC can affect ferroptosis by chelating iron ions besides targeting p65.

To deeply clarify the role of ferroptosis process in aspirin-triggered HCC cell death, we screened known ferroptosis-related genes and found that p65 significantly up-regulated the expression of SLC7A11 in hepatoma cells. SLC7A11 is considered as the central regulators of ferroptosis, and reduced levels of SLC7A11 are always regarded as markers of ferroptosis [53, 54]. Moreover, SLC7A11 has a well-established role in maintaining intracellular glutathione levels and protecting cells from oxidative-stress-induced ferroptosis, and SLC7A11 is frequently overexpressed in cancers [55–57]. Furthermore, as p65 functioned as a transcription factor, we demonstrated that p65 could bind on the core promoter region of *SLC7A11* promoter and activate the transcription of SLC7A11. Thus, aspirin down-regulated the expression of SLC7A11 through p65, resulting in ferroptosis. In addition, we found that aspirin/NF-κB p65-ferroptosis axis also worked in breast cancer and osteosarcoma. In this study, we screened the ferroptosis-related factors affected by p65. Both SLC7A11 and GPX4 were regulated by p65. Considering that the effect of p65 on SLC7A11 expression was stronger than that of GPX4, we investigated the effect of SLC7A11 on aspirin-mediated ferroptosis in liver cancer. It has been reported that GPX4 as a p65-regulated factor is involved in the progression of ferroptosis [58]. Potentially, aspirin might enhance ferroptosis through p65-mediated GPX4 as well. Thus, we conclude that aspirin induces ferroptosis through inhibiting NF-κB p65-activated SLC7A11 transcription in cancers.

Accordingly, we concerned whether aspirin inhibited the growth of cancer cells through modulating p65-induced ferroptosis. Interestingly, we validated that aspirin suppressed the proliferation of hepatoma cells through p65-mediated ferroptosis, which was also confirmed in MCF7 and U2OS cell lines. The in vivo tumorigenicity assays demonstrated that the treatment with aspirin sharply suppressed the growth of liver cancer and enhanced ferroptosis in mice, which could be reversed by overexpression of p65. In function, we found that co-treatment with aspirin and erastin could inhibit the growth of cancers through inducing ferroptosis, which may be a potential strategy for cancer therapy. Therefore, we conclude that aspirin triggers ferroptosis by restricting NF-κB-activated SLC7A11 to depress the growth of tumor. Our finding provides new insights into the mechanism by which aspirin regulates ferroptosis in hepatocarcinogenesis.

In conclusion, we uncover that aspirin induces ferroptosis in cancer cells via NF-κB p65/SLC7A11 signaling, leading to the inhibition of tumor growth. Aspirin is able to inhibit the activity of NF-κB p65. The p65 can activate the transcription of SLC7A11 through directly binding to the core region of *SLC7A11* promoter. Aspirin suppresses the expression of SLC7A11 by targeting NF-κB p65, resulting in the progression of ferroptosis. Aspirin significantly inhibits the growth of tumor by stimulating ferroptosis.

ACKNOWLEDGEMENTS

This study was supported by National Natural Science Foundation of China (No. 82103066, No. 81872184), China Postdoctoral Science Foundation (No. 2022M712389) and Tianjin Key Medical Discipline (Specialty) Construction Project (TJYXZDXK-009A).

AUTHOR CONTRIBUTIONS

YFW, JYF, and LNZ performed most of the experiments. MZ, XFW, YG, HFY, CYH, and HHZ performed some experiments. XDZ, GY, GWW and YFW designed the experiments. XDZ and YFW interpreted the results. XDZ and YFW wrote the paper with help from all authors.

ADDITIONAL INFORMATION

Supplementary information The online version contains supplementary material available at https://doi.org/10.1038/s41401-023-01062-1.

Competing interests: The authors declare no competing interests.

REFERENCES

1. Rizzollo F, More S, Vangheluwe P, Agostinis P. The lysosome as a master regulator of iron metabolism. Trends Biochem Sci. 2021;46:960–75.
2. Wang H, Cheng Y, Mao C, Liu S, Xiao D, Huang J, et al. Emerging mechanisms and targeted therapy of ferroptosis in cancer. Mol Ther. 2021;29:2185–208.
3. Gan B. Mitochondrial regulation of ferroptosis. J Cell Biol. 2021;220:e202105043.
4. Liu X, Zhang Y, Zhuang L, Olszewski K, Gan B. NADPH debt drives redox bankruptcy: SLC7A11/xCT-mediated cystine uptake as a double-edged sword in cellular redox regulation. Genes Dis. 2021;8:731–45.
5. Weaver K, Skouta R. The selenoprotein glutathione peroxidase 4: From molecular mechanisms to novel therapeutic opportunities. Biomedicines. 2022;10:891–910.
6. Li Z, Zhu Z, Liu Y, Liu Y, Zhao H. Function and regulation of GPX4 in the development and progression of fibrotic disease. J Cell Physiol. 2022;237:2808–24.

7. Yan R, Xie E, Li Y, Li J, Zhang Y, Chi X, et al. The structure of erastin-bound xCT-4F2hc complex reveals molecular mechanisms underlying erastin-induced ferroptosis. Cell Res. 2022;32:687–90.
8. Yang J, Mo J, Dai J, Ye C, Cen W, Zheng X, et al. Cetuximab promotes RSL3-induced ferroptosis by suppressing the Nrf2/HO-1 signalling pathway in KRAS mutant colorectal cancer. Cell Death Dis. 2021;12:1079–89.
9. Sun X, Ou Z, Chen R, Niu X, Chen D, Kang R, et al. Activation of the p62-Keap1-NRF2 pathway protects against ferroptosis in hepatocellular carcinoma cells. Hepatology. 2016;63:173–84.
10. Sun J, Zhou C, Zhao Y, Zhang X, Chen W, Zhou Q, et al. Quiescin sulfhydryl oxidase 1 promotes sorafenib-induced ferroptosis in hepatocellular carcinoma by driving EGFR endosomal trafficking and inhibiting NRF2 activation. Redox Biol. 2021;41:101942–60.
11. Marzouk HM, Ibrahim EA, Hegazy MA, Saad SS. Sustainable liquid chromatographic determination and purity assessment of a possible add-on triple-action over-the-counter pharmaceutical combination in COVID-19. Microchem J. 2022;178:107400–7.
12. Shvartsur R, Agam G, Uzzan S, Azab AN. Low-dose aspirin augments the anti-inflammatory effects of low-dose lithium in lipopolysaccharide-treated rats. Pharmaceutics. 2022;14:901–22.
13. Liu P, Wang ZH, Kang SS, Liu X, Xia Y, Chan CB, et al. High-fat diet-induced diabetes couples to Alzheimer's disease through inflammation-activated C/EBPβ/AEP pathway. Mol Psychiatry. 2022;27:3396–409.
14. Nguyen TNM, Sha S, Chen LJ, Holleczek B, Brenner H, Schöttker B. Strongly increased risk of gastric and duodenal ulcers among new users of low-dose aspirin: results from two large cohorts with new-user design. Aliment Pharmacol Ther. 2022;56:251–62.
15. Barry EL, Fedirko V, Jin Y, Liu K, Mott LA, Peacock JL, et al. Plasma metabolomics analysis of aspirin treatment and risk of colorectal adenomas. Cancer Prev Res (Philos). 2022;15:521–31.
16. Rezania MA, Eghtedari A, Taha MF, Ardekani AM, Javeri A. A novel role for aspirin in enhancing the reprogramming function of miR-302/367 cluster and breast tumor suppression. J Cell Biochem. 2022;123:1077–90.
17. Xu R, Yan Y, Zheng X, Zhang H, Chen W, Li H, et al. Aspirin suppresses breast cancer metastasis to lung by targeting anoikis resistance. Carcinogenesis. 2022;43:104–14.
18. Nguyen TNM, Chen LJ, Trares K, Stocker H, Holleczek B, Beyreuther K, et al. Long-term low-dose acetylsalicylic use shows protective potential for the development of both vascular dementia and Alzheimer's disease in patients with coronary heart disease but not in other individuals from the general population: results from two large cohort studies. Alzheimers Res Ther. 2022;14:75–88.
19. Simon TG, Ma Y, Ludvigsson JF, Chong DQ, Giovannucci EL, Fuchs CS, et al. Association between aspirin use and risk of hepatocellular carcinoma. JAMA Oncol. 2018;4:1683–90.
20. Yun B, Ahn SH, Yoon JH, Kim BK. Clinical indication of aspirin associated with reduced risk of liver cancer in chronic hepatitis B: a nationwide cohort study. Am J Gastroenterol. 2022;117:758–68.
21. Flossmann E, Rothwell PM. Effect of aspirin on long-term risk of colorectal cancer: consistent evidence from randomised and observational studies. Lancet. 2007;369:1603–13.
22. Algra AM, Rothwell PM. Effects of regular aspirin on long-term cancer incidence and metastasis: a systematic comparison of evidence from observational studies versus randomised trials. Lancet Oncol. 2012;13:518–27.
23. Liu YX, Feng JY, Sun MM, Liu BW, Yang G, Bu YN, et al. Aspirin inhibits the proliferation of hepatoma cells through controlling GLUT1-mediated glucose metabolism. Acta Pharmacol Sin. 2019;40:122–32.
24. Wu L, Luo Z, Liu Y, Jia L, Jiang Y, Du J, et al. Aspirin inhibits RANKL-induced osteoclast differentiation in dendritic cells by suppressing NF-κB and NFATc1 activation. Stem Cell Res Ther. 2019;10:375–85.
25. Jiang W, Yan Y, Chen M, Luo G, Hao J, Pan J, et al. Aspirin enhances the sensitivity of colon cancer cells to cisplatin by abrogating the binding of NF-κB to the COX-2 promoter. Aging (Albany NY). 2020;12:611–27.
26. Yoneda H, Miura K, Matsushima H, Sugi K, Murakami T, Ouchi K, et al. Aspirin inhibits Chlamydia pneumoniae-induced NF-kappa B activation, cyclo-oxygenase-2 expression and prostaglandin E2 synthesis and attenuates chlamydial growth. J Med Microbiol. 2003;52:409–15.
27. Murono S, Yoshizaki T, Sato H, Takeshita H, Furukawa M, Pagano JS. Aspirin inhibits tumor cell invasiveness induced by Epstein-Barr virus latent membrane protein 1 through suppression of matrix metalloproteinase-9 expression. Cancer Res. 2000;60:2555–61.
28. Yang G, Yuan Y, Yuan H, Wang J, Yun H, Geng Y, et al. Histone acetyltransferase 1 is a succinyltransferase for histones and non-histones and promotes tumorigenesis. EMBO Rep. 2021;22:e50967.
29. Zhao M, Bu Y, Feng J, Zhang H, Chen Y, Yang G, et al. SPIN1 triggers abnormal lipid metabolism and enhances tumor growth in liver cancer. Cancer Lett. 2020;470:54–63.
30. Lei G, Zhang Y, Koppula P, Liu X, Zhang J, Lin SH, et al. The role of ferroptosis in ionizing radiation-induced cell death and tumor suppression. Cell Res. 2020;30:146–62.
31. Arar NM, Pati P, Kashyap A, Khartchenko AF, Goksel O, Kaigala GV, et al. High-quality immunohistochemical stains through computational assay parameter optimization. IEEE Trans Biomed Eng. 2019;66:2952–63.
32. Yang LY, Luo Q, Lu L, Zhu WW, Sun HT, Wei R, et al. Increased neutrophil extracellular traps promote metastasis potential of hepatocellular carcinoma via provoking tumorous inflammatory response. J Hematol Oncol. 2020;13:3–17.
33. Memel ZN, Arvind A, Moninuola O, Philpotts L, Chung RT, Corey KE, et al. Aspirin use is associated with a reduced incidence of hepatocellular carcinoma: a systematic review and meta-analysis. Hepatol Commun. 2021;5:133–43.
34. Hui VW, Yip TC, Wong VW, Tse YK, Chan HL, Lui GC, et al. Aspirin reduces the incidence of hepatocellular carcinoma in patients with chronic hepatitis B receiving oral nucleos(t)ide analog. Clin Transl Gastroenterol. 2021;12:e00324.
35. Stockwell BR, Friedmann Angeli JP, Bayir H, Bush AI, Conrad M, Dixon SJ, et al. Ferroptosis: a regulated cell death nexus linking metabolism, redox biology, and disease. Cell. 2017;171:273–85.
36. Xu T, Ding W, Ji X, Ao X, Liu Y, Yu W, et al. Molecular mechanisms of ferroptosis and its role in cancer therapy. J Cell Mol Med. 2019;23:4900–12.
37. Jiang X, Stockwell BR, Conrad M. Ferroptosis: mechanisms, biology and role in disease. Nat Rev Mol Cell Biol. 2021;22:266–82.
38. Liang C, Zhang X, Yang M, Dong X. Recent progress in ferroptosis inducers for cancer therapy. Adv Mater. 2019;31:e1904197.
39. Yang Y, Luo M, Zhang K, Zhang J, Gao T, Connell DO, et al. Nedd4 ubiquitylates VDAC2/3 to suppress erastin-induced ferroptosis in melanoma. Nat Commun. 2020;11:433–46.
40. Liao D, Zhong L, Duan T, Zhang RH, Wang X, Wang G, et al. Aspirin suppresses the growth and metastasis of osteosarcoma through the NF-κB pathway. Clin Cancer Res. 2015;21:5349–59.
41. Wang T, Fu X, Jin T, Zhang L, Liu B, Wu Y, et al. Aspirin targets P4HA2 through inhibiting NF-κB and LMCD1-AS1/let-7g to inhibit tumour growth and collagen deposition in hepatocellular carcinoma. EBioMedicine. 2019;45:168–80.
42. Yuan Y, Yuan HF, Geng Y, Zhao LN, Yun HL, Wang YF, et al. Aspirin modulates 2-hydroxyisobutyrylation of ENO1K281 to attenuate the glycolysis and proliferation of hepatoma cells. Biochem Biophys Res Commun. 2021;560:172–8.
43. Deng N, Ye Y, Wang W, Li L. Dishevelled interacts with p65 and acts as a repressor of NF-κB-mediated transcription. Cell Res. 2010;20:1117–27.
44. Białas N, Müller EK, Epple M, Hilger I. Silica-coated calcium phosphate nanoparticles for gene silencing of NF-κB p65 by siRNA and their impact on cellular players of inflammation. Biomaterials. 2021;276:121013–25.
45. Mudipalli A, Li Z, Hromchak R, Bloch A. NF-kappaB (p65/RelA) as a regulator of TNFalpha-mediated ML-1 cell differentiation. Leukemia. 2001;15:808–13.
46. Lee TY, Hsu YC, Tseng HC, Yu SH, Lin JT, Wu MS, et al. Association of daily aspirin therapy with risk of hepatocellular carcinoma in patients with chronic hepatitis B. JAMA Intern Med. 2019;179:633–40.
47. Yang G, Wang Y, Feng J, Liu Y, Wang T, Zhao M, et al. Aspirin suppresses the abnormal lipid metabolism in liver cancer cells via disrupting an NF-κB-ACSL1 signaling. Biochem Biophys Res Commun. 2017;486:827–32.
48. Yang WS, Stockwell BR. Ferroptosis: death by lipid peroxidation. Trends Cell Biol. 2016;26:165–76.
49. Dixon SJ, Lemberg KM, Lamprecht MR, Skouta R, Zaitsev EM, Gleason CE, et al. Ferroptosis: an iron-dependent form of nonapoptotic cell death. Cell. 2012;149:1060–72.
50. Wang L, Liu Y, Du T, Yang H, Lei L, Guo M, et al. ATF3 promotes erastin-induced ferroptosis by suppressing system Xc. Cell Death Differ. 2020;27:662–75.
51. Giridharan S, Srinivasan M. Mechanisms of NF-κB p65 and strategies for therapeutic manipulation. J Inflamm Res. 2018;11:407–19.
52. Bowie AG, Moynagh PN, O'Neill LA. Lipid peroxidation is involved in the activation of NF-kappaB by tumor necrosis factor but not interleukin-1 in the human endothelial cell line ECV304. Lack of involvement of H2O2 in NF-kappaB activation by either cytokine in both primary and transformed endothelial cells. J Biol Chem. 1997;272:25941–50.
53. Fang X, Cai Z, Wang H, Han D, Cheng Q, Zhang P, et al. Loss of cardiac ferritin h facilitates cardiomyopathy *via* Slc7a11-mediated ferroptosis. Circ Res. 2020;127:486–501.
54. Dong H, Qiang Z, Chai D, Peng J, Xia Y, Hu R, et al. Nrf2 inhibits ferroptosis and protects against acute lung injury due to intestinal ischemia reperfusion via regulating SLC7A11 and HO-1. Aging (Albany NY). 2020;12:12943–59.

55. Lang X, Green MD, Wang W, Yu J, Choi JE, Jiang L, et al. Radiotherapy and immunotherapy promote tumoral lipid oxidation and ferroptosis *via* synergistic repression of SLC7A11. Cancer Discov. 2019;9:1673–85.
56. Koppula P, Zhuang L, Gan B. Cystine transporter SLC7A11/xCT in cancer: ferroptosis, nutrient dependency, and cancer therapy. Protein Cell. 2021;12:599–620.
57. Zhang W, Sun Y, Bai L, Zhi L, Yang Y, Zhao Q, et al. RBMS1 regulates lung cancer ferroptosis through translational control of SLC7A11. J Clin Invest. 2021; 131:e152067.
58. Bersuker K, Hendricks JM, Li Z, Magtanong L, Ford B, Tang PH, et al. The CoQ oxidoreductase FSP1 acts parallel to GPX4 to inhibit ferroptosis. Nature. 2019;575:688–92.